

Article

Strain Modulation of Electronic Properties in Monolayer SnP₂S₆ and GeP₂S₆

Junlei Zhou ¹, Yuzhou Gu ¹, Yue-E Xie ¹, Fen Qiao ¹, Jiaren Yuan ^{2,*}, Jingjing He ³, Sake Wang ⁴ , Yangsheng Li ^{2,*} and Yangbo Zhou ^{2,*}¹ School of Physics and Electronic Engineering, Jiangsu University, Zhenjiang 212013, China² School of Physics and Materials Science, Nanchang University, Nanchang 330031, China³ College of Information Science and Technology, Nanjing Forestry University, Nanjing 210037, China⁴ School of Science, Jinling Institute of Technology, Nanjing 211169, China

* Correspondence: jryuan@ncu.edu.cn (J.Y.); ysli@ncu.edu.cn (Y.L.); yangbozhou@ncu.edu.cn (Y.Z.)

Abstract: In recent years, two-dimensional (2D) materials have attracted significant attention due to their distinctive properties, including exceptional mechanical flexibility and tunable electronic properties. Via the first-principles calculation, we investigate the effect of strain on the electronic properties of monolayer SnP₂S₆ and GeP₂S₆. We find that monolayer SnP₂S₆ is an indirect bandgap semiconductor, while monolayer GeP₂S₆ is a direct bandgap semiconductor. Notably, under uniform biaxial strains, SnP₂S₆ undergoes an indirect-to-direct bandgap transition at 4.0% biaxial compressive strains, while GeP₂S₆ exhibits a direct-to-indirect transition at 2.0% biaxial tensile strain. The changes in the conduction band edge can be attributed to the high-symmetry point Γ being more sensitive to strain than K. Thus, the relocation of the conduction band and valence band edges in monolayer SnP₂S₆ and GeP₂S₆ induces a direct-to-indirect and indirect-to-direct bandgap transition, respectively. Consequently, the strain is an effective band engineering scheme which is crucial for the design and development of next-generation nanoelectronic and optoelectronic devices.

Keywords: monolayer semiconductor; bandgap; electronic structure; biaxial strain; DFT calculations

Citation: Zhou, J.; Gu, Y.; Xie, Y.-E.; Qiao, F.; Yuan, J.; He, J.; Wang, S.; Li, Y.; Zhou, Y. Strain Modulation of Electronic Properties in Monolayer SnP₂S₆ and GeP₂S₆. *Inorganics* **2023**, *11*, 301. <https://doi.org/10.3390/inorganics11070301>

Academic Editor: Antonino Gulino

Received: 3 June 2023

Revised: 10 July 2023

Accepted: 13 July 2023

Published: 15 July 2023



Copyright: © 2023 by the authors. Licensee MDPI, Basel, Switzerland. This article is an open access article distributed under the terms and conditions of the Creative Commons Attribution (CC BY) license (<https://creativecommons.org/licenses/by/4.0/>).

1. Introduction

Two-dimensional (2D) materials, such as graphene [1,2], have attracted significant interest because of their exotic physical properties and potential application in nanoelectronic and optoelectronic devices [3]. However, graphene is a semimetal with zero bandgaps [4], and the absence of a bandgap will limit its application in nanoscale optoelectronic and cutting-edge ultra-fast electronic devices of the next generation [5]. Hence, the exploration of 2D materials with appropriate bandgaps is of great importance for device applications. The transition metal dichalcogenides (TMDs) [6], hexagonal boron nitride (b-BN) [7], germanene (2D germanium) [8], and metal halogenides [9,10], among others, have garnered substantial interest in the realms of materials science, microelectronics, physics, and related fields. Among these encouraging candidates, 2D nanoporous metal chalcogen phosphates MP₂S₆ (M = metal, X = S, Se) including SnP₂S₆ and GeP₂S₆ have also captured considerable attention because of their moderate-to-wide bandgaps ranging from 1.2 eV to 3.5 eV [11]. Similar to TMDCs, SnP₂S₆ and GeP₂S₆ share properties of typical 2D materials [12], with a weak van der Waals interlayer interaction [13], a high surface-to-volume ratio and excellent optical properties [14]. Moreover, metal chalcogen phosphates MP₂X₆ have rich properties, including topological magnetism [15], ferroelectric ordering [16], photocatalytic properties [17], and H₂ storage and Li intercalation for batteries [11]. For example, monolayer SnP₂S₆ is an indirect bandgap semiconductor with high carrier mobility and with a bandgap of 1.1 eV, while monolayer GeP₂S₆ is a direct bandgap semiconductor with a bandgap of 1.06 eV, which shows promising potential in electronic and photoelectronic applications [18,19]. Furthermore, SnP₂S₆ and GeP₂S₆ are 2D porous materials that are

important as membranes, adsorbents, catalysts, and in other chemical applications. The novel physical properties of 2D nanoporous metal chalcogen phosphate materials have the potential to expand the range of applications in nanoelectronics [11]. He et al. reported that SnP_2S_6 exhibits nonlinear optical characteristics with significant nonresonant second harmonic generation, which lays the foundation for developing novel optoelectronic devices [20].

The development of 2D materials has attracted considerable attention owing to its unique attributes, including tunable electronic properties. Strain is a promising avenue for tuning the electric properties of two-dimensional materials [21,22]. Theoretical studies have shown that transition metal disulfide compounds (TMDs) are sensitive to strain [23], and strain engineering can shift the conduction band minimum (CBM) and valence band maximum (VBM) [23–26]. It has been reported that the application of tensile strain can lead to a narrowing of the bandgap in MoS_2 in a monolayer system [27,28]. Moreover, the direct-to-indirect bandgap transition can occur in monolayer MoS_2 with 6% tensile strain [29]. The strain-tuned electronic properties in 2D materials have significant implications for the development of next-generation nanoelectronic and optoelectronic devices [30–32]. Furthermore, studies have also investigated the effects of applying pressure to layered SnP_2S_6 and GeP_2S_6 . The transition from a semiconductor to a metal has been reported in layered SnP_2S_6 and GeP_2S_6 [33]. We will now shift our research focus towards investigating the effects of biaxial strain on monolayer SnP_2S_6 and GeP_2S_6 . The metal chalcogen phosphates SnP_2S_6 and GeP_2S_6 with intrinsic nanoporous structures possess excellent mechanical performance, and are expected to be able to effectively tune the electronic properties under strain [34].

In this study, we investigated the ground-state monolayers of SnP_2S_6 and GeP_2S_6 , revealing that monolayer SnP_2S_6 and GeP_2S_6 are thermodynamically stable. Monolayer SnP_2S_6 and GeP_2S_6 are indirect bandgap semiconductors with a 1.35 eV gap and a direct bandgap semiconductor with a gap of 1.06 eV in equilibrium, respectively. Additionally, we modulated their electronic structures by applying strain from 6% compression to 6% tension. When a 4% biaxial compression (BC) strain was applied to the monolayer SnP_2S_6 , it transformed from an indirect bandgap semiconductor to a direct bandgap semiconductor. Similarly, when a 2% biaxial tension (BT) strain was applied to the monolayer GeP_2S_6 , it transitioned from a direct bandgap semiconductor to an indirect bandgap semiconductor. These results provide valuable insights into the strain engineering in tuning the electronic structures of the monolayer systems.

2. Result and Discussion

SnP_2S_6 and GeP_2S_6 are members of the family of novel 2D metal thiophosphates. These monolayers are characterized by space group P312 and contain one metal cation (Sn or Ge) and one anionic $[\text{P}_2\text{S}_6]^{4-}$ unit, as illustrated in Figure 1a,b [34]. The metal cation undergoes coordination with six sulfur (S) atoms, thereby forming a hexahedral structure, whereas each phosphorus (P) atom is coordinated with three sulfur atoms in a tetrahedral arrangement, as depicted in Figure 1b. The monolayer SnP_2S_6 and GeP_2S_6 exhibit optimized lattice parameters of 6.13 Å and 5.99 Å, respectively, which is consistent with the previous result [35]. The optimized lattice parameters reflect the equilibrium distances between the atoms in the monolayers, providing insights into their structural stability and interatomic bonding characteristics. Undoubtedly, the stability of materials is a crucial consideration in materials science and applications. Therefore, we employed the finite displacement method to calculate the phonon spectra of monolayer SnP_2S_6 and monolayer GeP_2S_6 using a $4 \times 4 \times 1$ supercell via phonopy [36]. Notably, as shown in Figure 2, no imaginary phonon frequencies were found throughout the entire Brillouin zone for monolayer GeP_2S_6 and the imaginary frequency near Γ is negligible for monolayer SnP_2S_6 , indicating that both structures are stable. In fact, monolayer SnP_2S_6 has been experimentally synthesized via chemical vapor transport technique along with the mechanical exfoliation method and used for preparing optoelectronic devices [37].

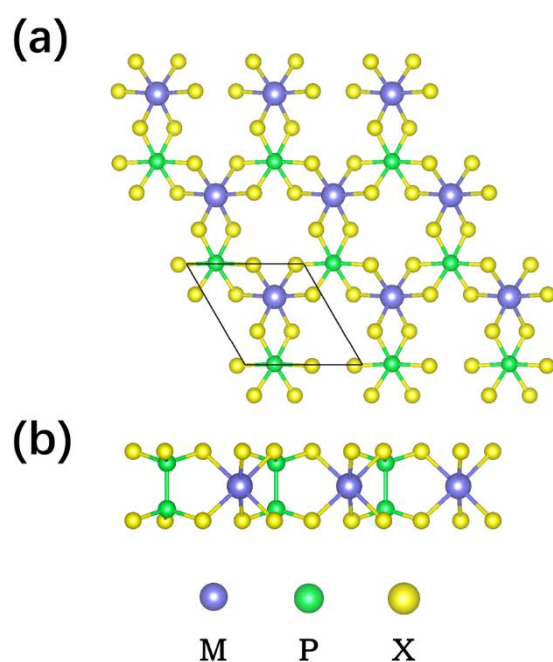


Figure 1. (a) Top and (b) side views of the monolayer MP_2S_6 are shown in the figure. The M (M = Sn, Ge) atoms, P atoms, and S atoms are represented by blue, green, and yellow spheres, respectively.

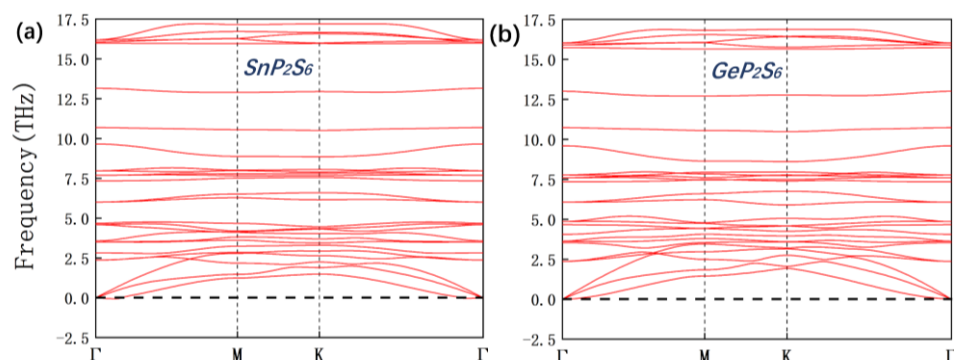


Figure 2. (a) Phonon spectrum of monolayer SnP_2S_6 . (b) Phonon spectrum of monolayer GeP_2S_6 .

Biaxial strain is employed in this study to investigate the impact of strain on the electronic properties of monolayer SnP_2S_6 and GeP_2S_6 . Biaxial strain is defined as follows:

$$\delta = \frac{\Delta a}{a_0} \quad (1)$$

where a_0 represents the optimized lattice constant when the structure is unstrained and Δa denotes the variation in the lattice constant after the application of a specific strain in the xy plane. Electronic property calculations are conducted over a range of δ values spanning from -6% to $+6\%$, representing the percentage change in the lattice constant. The negative value of δ indicates compressive strain, where the lattice is compressed along the xy plane. Conversely, the positive sign refers to tensile strain, where the lattice is stretched along the xy plane. By systematically varying the strain within this range, we were able to investigate the influence of strain on the electronic properties of the monolayers. This analysis provides valuable insights into the strain-dependent behavior of the materials, including changes in band structure, bandgap, and other electronic characteristics. The comprehensive range of strain values allows us to explore the full spectrum of electronic responses in SnP_2S_6 and GeP_2S_6 , enhancing our understanding of their potential applications in strain-engineered devices and electronic systems.

The electronic band structures of monolayer SnP_2S_6 and GeP_2S_6 structures under biaxial strain are investigated. Our calculations reveal that the total energy of the system exhibits a weak dependence on the applied biaxial strain, as depicted in Figure 3. The calculated total energy for the relaxed monolayer structures of SnP_2S_6 and GeP_2S_6 is determined to be -42.6808 eV and -42.4794806 eV, respectively. The maximum change in total energy is only around 0.5 eV and 0.6 eV within the considered strain range. While the impact of strain on total energy may appear to be minimal, it plays a significant role in determining the material properties. Even slight changes in total energy can result in noticeable modifications to the electronic band structure, bandgap, and other electronic characteristics of the monolayers. Thus, comprehending the influence of strain on total energy is vital for the precise prediction and control of the electronic behavior exhibited by SnP_2S_6 and GeP_2S_6 under varying strain conditions.

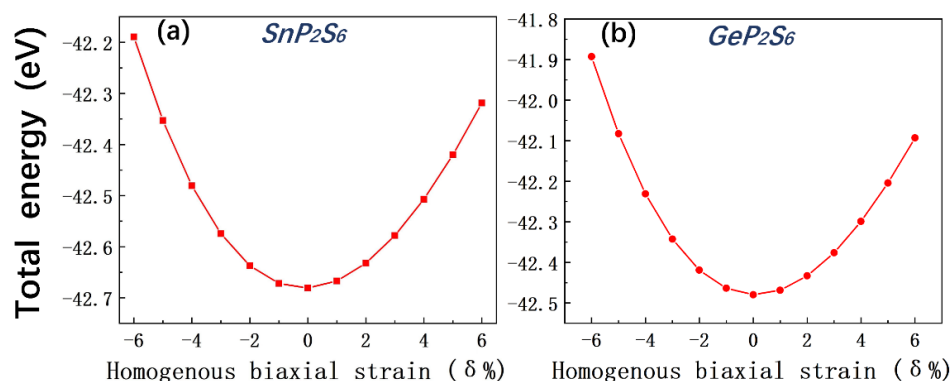


Figure 3. (a) Total energy vs. strain in monolayer SnP_2S_6 . (b) Total energy vs. strain in monolayer GeP_2S_6 .

The electronic band structure of the unstrained SnP_2S_6 is presented in Figure 4a, where the VBM is located at the K point, while the CBM is located at the Γ point, with an indirect bandgap of 1.346 eV, which is consistent with previous calculation results (1.35 eV) [34]. The contribution of different orbitals to the VBM and CBM are investigated by calculating the orbitals' resolved density of states. S - p orbitals contribute mostly to the VBM, while Sn - s orbitals have the highest contribution to the CBM, along with a minor contribution from S - p orbitals, as illustrated in Figure 4a. To further explore the effect of homogeneous biaxial strain on the electronic structure of SnP_2S_6 , we examined the impact of a 4.0% BC strain. Under this strain condition, a notable shift in the CBM is observed from the Γ point to the K point, while the VBM remains localized at the K point. This shift results in an intriguing indirect-to-direct bandgap transition, as depicted in Figure 4b. The findings emphasize the significant role of strain engineering in modifying the electronic properties of SnP_2S_6 . By manipulating the strain, it becomes possible to tailor the band structure and control the bandgap characteristics of the material. This newfound capability holds immense promise for the development of strain-tunable electronic devices, as well as for applications in fields such as optoelectronics and energy harvesting. Importantly, the information obtained from this study contributes to a deeper understanding of the underlying mechanisms governing the electronic behavior of SnP_2S_6 under strain, providing valuable insights for future research endeavors in this field.

Similarly, we investigated the electronic structure of the unstrained GeP_2S_6 and strained system, as illustrated in Figure 4c,d. It is worth noting that the VBM and CBM of the unstrained GeP_2S_6 monolayer are both located at the K point, indicating a direct bandgap semiconductor with a bandgap of 1.06 eV, which is consistent with the results of previous studies employing the same methodology (1.06 eV) [19]. As depicted in Figure 4c, the majority of the orbital contribution to the VBM results from S - p orbitals, whereas Ge - s orbital dominates the CBM along with a minor contribution from S - p orbitals. Under the influence of a 2.0% BT strain, the CBM experienced a significant shift from the K point

to the Γ point, while the VBM remained unchanged at the K point. This strain-induced phenomenon led to an intriguing transition from a direct bandgap to an indirect bandgap in the material. By manipulating the strain, researchers can fine-tune the electronic properties of GeP_2S_6 , enabling the design and development of strain-tailored devices with enhanced performance. In contrast, molybdenum disulfide (MoS_2) undergoes a semiconductor-to-metal transition under significantly large strains [38], exhibiting a pronounced shift in the valence band maximum from the high-symmetry point K to the Γ point when the tensile strain reaches 6%. This transition leads to a transformation of the initial direct bandgap into an indirect one [24]. Therefore, compared to MoS_2 , both systems investigated in this study exhibit a stronger strain-tuning effect under a relatively small strain, which holds significant implications for researchers studying two-dimensional and nanoscale electronic materials.

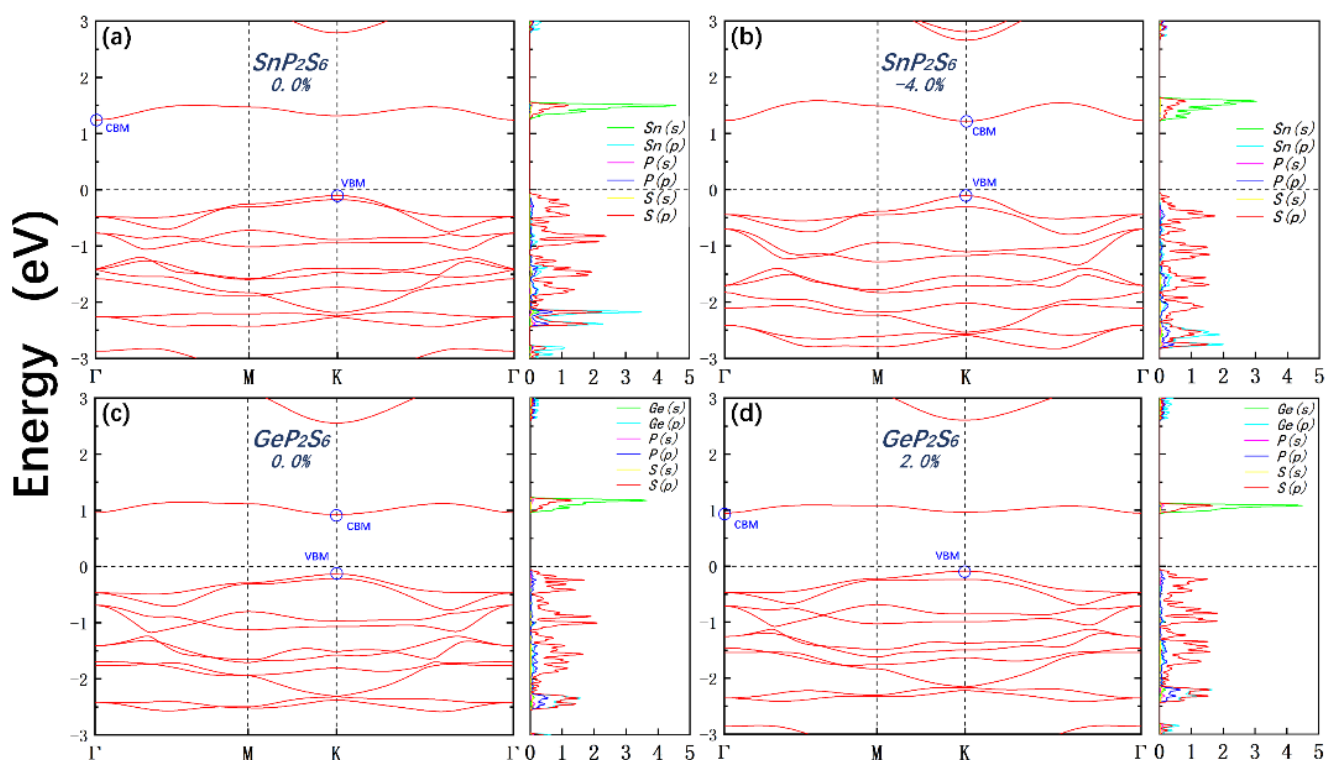


Figure 4. (a,b) Monolayer SnP_2S_6 electronic band structure and angular-momentum resolved density of states at 0.0% and 4.0% BC strain, respectively. (c,d) The monolayer GeP_2S_6 at 0.0% and 2.0% BT strain.

In order to gain deeper insights into the orbital contributions to the band structure, we conducted an analysis of the projected band structure in the absence of strain. Our calculations reveal distinct orbital contributions to the conduction and valence band edges in both materials. It is evident that the conduction band edge of system SnP_2S_6 is primarily contributed by Sn-s orbitals, with additional small contributions from S- p_z orbitals and a small contribution from S- p_x/p_y orbitals, while the valence band edge is predominantly attributed to the S- p_x orbital with a small contribution from the S- p_y orbital in Figure 5a–d. Similarly, the conduction band edge of the GeP_2S_6 monolayer is primarily influenced by the Ge-s orbital, while the valence band edge is predominantly affected by the S- p_x orbital with a small contribution from S- p_z orbitals, as depicted in Figure 6a–d. This analysis provides valuable insights into the orbital characteristics responsible for the electronic properties of SnP_2S_6 and GeP_2S_6 . Understanding the specific orbital contributions aids the elucidation of the underlying mechanisms that govern the material’s electronic behavior and facilitates the design and optimization of electronic devices based on these materials.

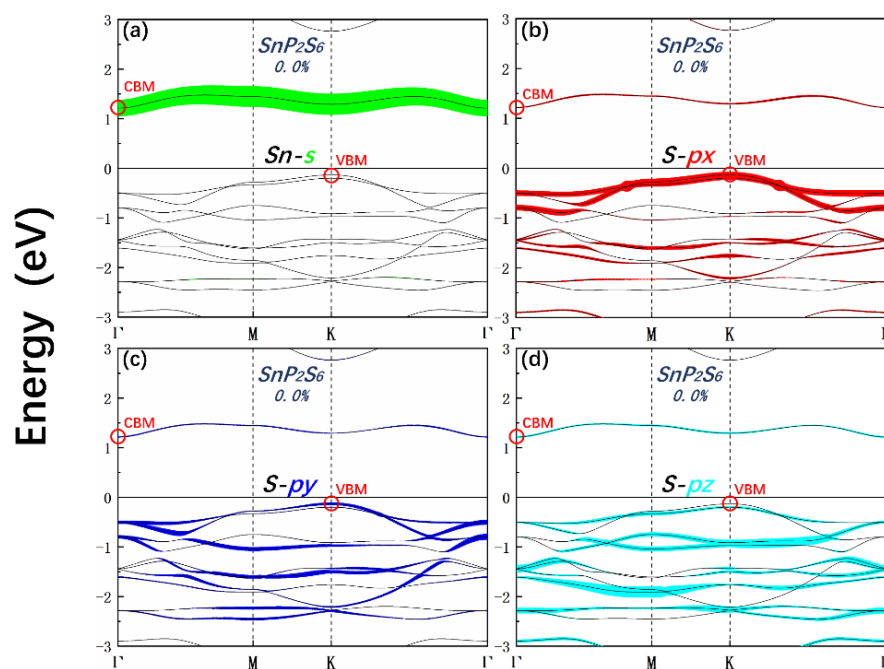


Figure 5. The orbital-resolved band structure of SnP_2S_6 under unstrained conditions for the Sn-s (a), S-px (b), S-py (c), and S-pz (d) orbitals is as follows: Red circles represent the corresponding VBM and CBM in the band structures.

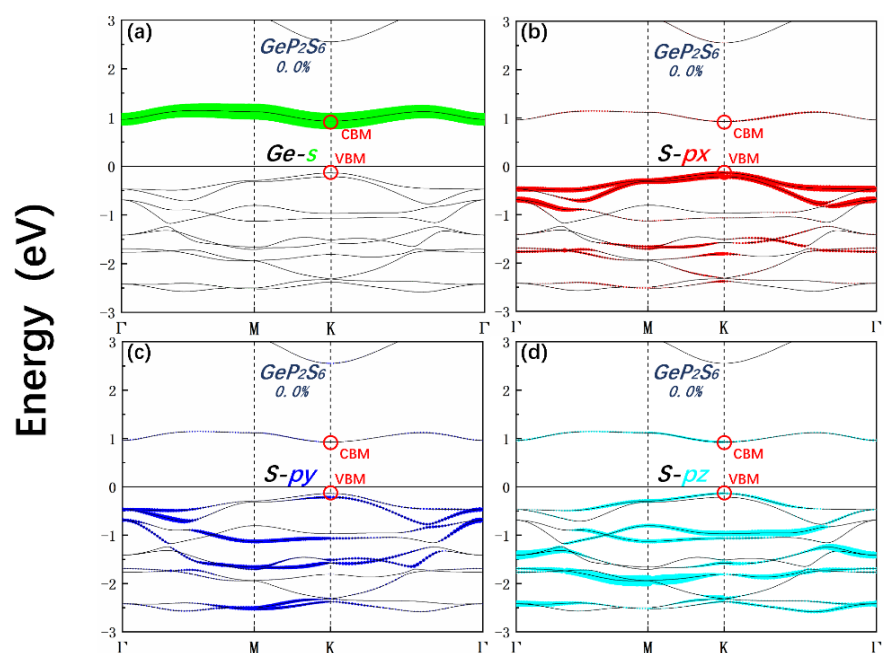


Figure 6. The orbital-resolved band structure of GeP_2S_6 under unstrained conditions for the Ge-s (a), S-px (b), S-py (c), and S-pz (d) orbitals is as follows: Red circles represent the corresponding VBM and CBM in the band structures.

According to Figure 4a–d, the conversion from an indirect to direct bandgap for monolayer SnP_2S_6 and the transformation from a direct to indirect bandgap for monolayer GeP_2S_6 is primarily caused by the shift in the conduction band minimum. To further investigate this phenomenon, we plotted the variation in the energy of the conduction band edge state at the Γ point (CB- Γ) and at the K point (CB-K) as a function of strain as depicted in Figure 7a,b. It is evident that both systems exhibit an approximately linear decrease in

energy with increasing tensile strain and an increase in energy with increasing compressive strain, for both the Γ and K points. The high-symmetry point Γ exhibits a higher rate under strain as compared to the K point, indicating the band edge near Γ point is more sensitive to strain. Hence, the positional relationship the energy bands at Γ and K points reverses under certain strain. In the case of system SnP_2S_6 , when the applied strain is less than -4% , $E_{\text{CB-}\Gamma}$ is smaller than $E_{\text{CB-K}}$ located at K. However, when the applied strain exceeds -4% , $E_{\text{CB-}\Gamma}$ becomes larger than $E_{\text{CB-K}}$, and the CBM shifts to the Γ point. Conversely, in the case of GeP_2S_6 , when the strain is less than 1% , $E_{\text{CB-}\Gamma}$ is larger than $E_{\text{CB-K}}$, and the CBM is located at the K point. However, when the strain exceeds 2% , $E_{\text{CB-}\Gamma}$ becomes smaller than $E_{\text{CB-K}}$, and the CBM shifts to the Γ point. These findings indicate that the strain-induced changes in the position of the CBM play a crucial role in determining the bandgap characteristics of SnP_2S_6 and GeP_2S_6 . The precise control of strain allows for the manipulation of the electronic properties of these materials, providing opportunities for tailoring their behavior and optimizing their performance in various electronic applications.

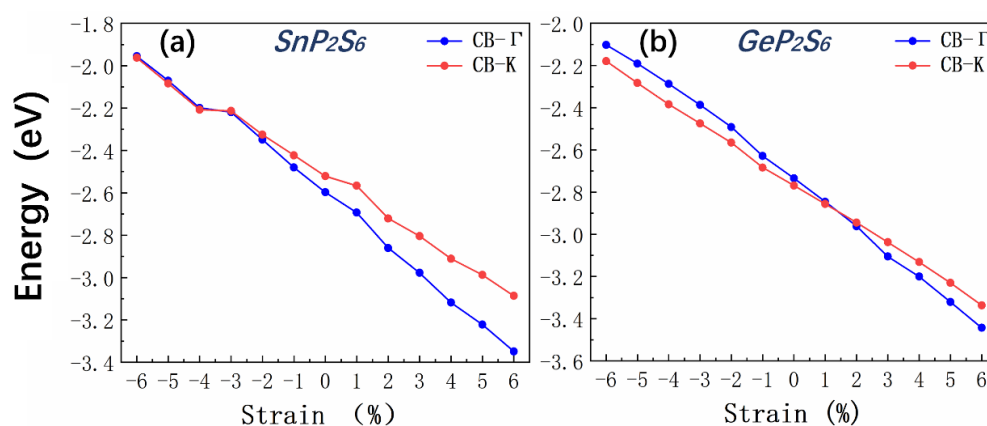


Figure 7. The variation in CBM energy at the Γ point (CB- Γ) and at the K point (CB-K) with strain for SnP_2S_6 (a) and GeP_2S_6 (b).

Figure 7 reveals that the two systems have the same energy level shift tendency. The energy level of the Γ point and K point for the conduction band in both materials increases with increasing compressive strain and decreases with increasing tensile strain. Furthermore, the energy level of the Γ point for the conduction band in both materials is more sensitive than that of the K point. The difference is that the energy band types of monolayer SnP_2S_6 and monolayer GeP_2S_6 at zero strain are inconsistent. Monolayer SnP_2S_6 with an indirect bandgap will transform into a direct bandgap semiconductor; since the Γ point is more sensitive, the energy of the Γ point rises faster than that of the K point, and the energy positions are reversed at 2% compressive strain. However, monolayer GeP_2S_6 with a direct bandgap will transform into an indirect bandgap semiconductor since the energy of the Γ point drops faster than that of the K point, and the energy positions are reversed at 4% tensile strain. Furthermore, we believe these insights can be applied to other 2D materials because other 2D systems also have similar phenomenon with different strain sensitivities at different k points. Therefore, these insights provide crucial references and guidance for researchers exploring strain modulation effects in other two-dimensional materials.

Furthermore, we investigated the modulation of the bandgap as a function of strain along distinct symmetry axes, namely K-K and K- Γ . Analyzing the bandgap behavior, we observed that in the case of SnP_2S_6 , when the strain is less than -4% , the bandgaps along the K-K and K- Γ directions exhibit remarkable proximity, suggesting a nearly degenerate nature. This finding implies that the band structure is relatively insensitive to strain in this range. However, as the strain exceeds -4% , an intriguing trend emerges. The disparity between the bandgaps along K-K and K- Γ becomes increasingly prominent, as depicted in Figure 8a. Specifically, we found that the bandgap undergoes only subtle changes under

compressive strain but exhibits significant variations under tensile strain. This strain-induced modification in the bandgap characteristics highlights the potential for tailoring the electronic properties of SnP_2S_6 through strain engineering. On the other hand, our investigation of monolayer GeP_2S_6 revealed a different pattern. Under compressive strain, the distinction between the bandgaps along the K-K and K- Γ directions is relatively more pronounced compared to that of SnP_2S_6 . This implies that the band structure of GeP_2S_6 is more sensitive to compressive strain, leading to a significant difference in the bandgap behavior between these two symmetry directions. Figure 8b illustrates the substantial changes in the bandgap under both compressive and tensile strains, further highlighting the potential for strain engineering in manipulating the electronic properties of GeP_2S_6 . By precisely controlling the strain, researchers can fine-tune the bandgap characteristics of SnP_2S_6 and GeP_2S_6 , enabling the development of tailored electronic devices with enhanced performance. The ability to manipulate the band structure through strain engineering opens up new avenues for exploring novel device concepts and applications. Furthermore, our study contributes to the broader understanding of strain-dependent phenomena in 2D materials. By unraveling the intricate relationship between strain and bandgap variations, we gain deeper insights into the underlying mechanisms governing the electronic behavior of these materials. This knowledge serves as a valuable foundation for future research endeavors in the field of strain engineering and paves the way for the discovery and optimization of other 2D materials with tailored electronic properties. The distinct variations observed under different strain conditions offer exciting possibilities for bandgap engineering and the design of advanced electronic and optoelectronic devices.

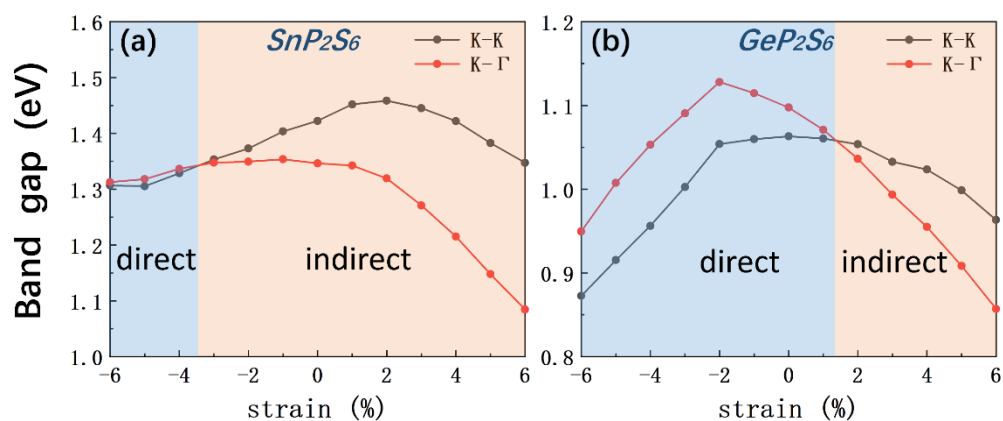


Figure 8. (a) Variations in bandgap along the high-symmetry directions K-K and K- Γ in SnP_2S_6 . (b) Bandgap fluctuations along the high-symmetry directions K-K and K- Γ in GeP_2S_6 .

In addition, we have also investigated the electronic structures considering spin-orbit coupling (SOC). When SOC is included as shown in Figure 9, the band splitting is observed for some bands, especially at high-symmetry points in both systems. However, no noticeable change in the electronic properties near the band edges is observed. The band structures with SOC are highly similar to those without SOC. Specifically, an indirect bandgap semiconductor with a bandgap of 1.35 eV remains for SnP_2S_6 with SOC, while for GeP_2S_6 with SOC, a direct bandgap semiconductor with a bandgap of 1.06 eV remains. Moreover, the positions of the conduction band minimum and valence band maximum remain the same as those without SOC. Based on these results, we conclude that the inclusion of SOC does not significantly affect the electronic structures as discussed in the previous sections. Therefore, SOC was not considered in the previous analysis.

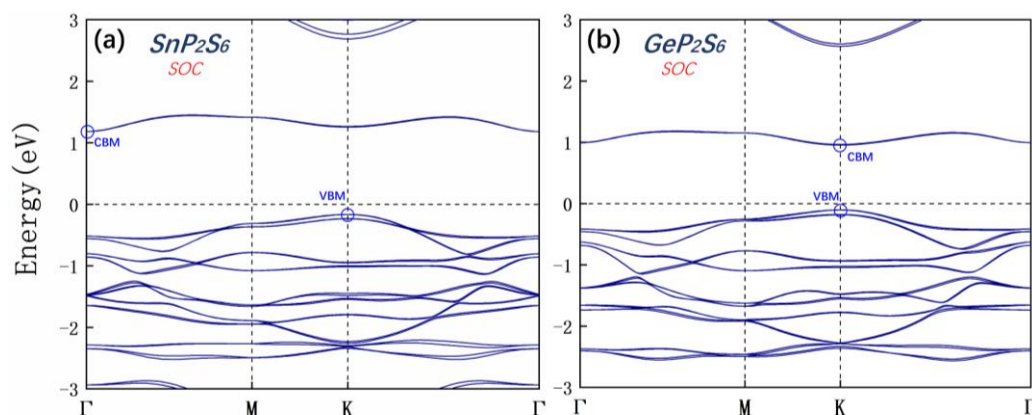


Figure 9. (a) Monolayer SnP_2S_6 electronic band structure with SOC. (b) Monolayer SnP_2S_6 electronic band structure with SOC.

3. Calculation Method

Density functional theory (DFT) [39] calculation was performed to investigate the electronic properties of monolayer metal chalcogen phosphates of SnP_2S_6 and GeP_2S_6 using the Vienna ab initio simulation package (VASP) [40]. The projector-augmented wave method was adopted with a cutoff energy of 450 eV [40]. The Perdew–Burke–Ernzerhof (PBE) [41] exchange–correlation function, based on the generalized gradient approximation (GGA), was employed in this study. To minimize the number of interactions between vertically periodic layers, a vacuum layer of 25 Å was set in the z direction for the monolayer structures. A $15 \times 15 \times 1$ Monkhorst–Pack k-grid mesh was employed for Brillouin zone sampling. The phonon spectra of monolayer SnP_2S_6 and monolayer GeP_2S_6 were calculated using the finite displacement method with a low repetition rate of a $4 \times 4 \times 1$ supercell. The atomic positions were iteratively optimized until the magnitude of the Hellmann–Feynman forces acting on all atoms was below $0.01 \text{ eV}/\text{Å}$, ensuring the convergence of the system.

4. Conclusions

In summary, we have conducted a comprehensive investigation on the electronic properties of monolayer SnP_2S_6 and GeP_2S_6 under biaxial strain. The results demonstrate that the monolayer SnP_2S_6 with an indirect bandgap of 1.346 eV undergoes a transition from an indirect to a direct bandgap under 4.0% uniform BC strain. Additionally, we report a direct-to-indirect bandgap transition in the monolayer semiconductor GeP_2S_6 under a uniform BT strain of 2.0%. The transition occurs because the high-symmetry point Γ is more sensitive to strain than K. Overall, our findings highlight the significant role of strain engineering in modulating the electronic properties of monolayer SnP_2S_6 and GeP_2S_6 . The ability to induce bandgap transitions through strain opens up avenues for designing innovative devices with enhanced performance and functionality. Further exploration of strain effects and the development of strain engineering techniques will undoubtedly contribute to the advancement of next-generation electronic and optoelectronic devices based on these materials.

Author Contributions: Conceptualization, J.Z.; methodology, Y.G.; validation, Y.-E.X. and F.Q.; formal analysis, J.Z. and Y.G.; investigation, J.Z. and Y.G.; resources, J.H.; data curation, J.Z.; writing—original draft, J.Z. and J.Y.; writing—review and editing, S.W., Y.L. and Y.Z.; supervision, J.Y., Y.L. and Y.Z. All authors have read and agreed to the published version of the manuscript.

Funding: This work was supported by the National Natural Science Foundation of China (Nos. 62264010, 12264026, 12004142, 62201268), the Natural Science Foundation of Jiangxi Province, China (Nos. 20212BAB211023, 20224BAB211013) and the Innovation and Entrepreneurship Leading Talent Plan of Jiangxi Province (Nos. Jxsq2023101068).

Data Availability Statement: Not applicable.

Conflicts of Interest: The authors declare no conflict of interest.

References

1. Geim, A.K.; Novoselov, K.S. The rise of graphene. *Nat. Mater.* **2007**, *6*, 183–191. [[CrossRef](#)] [[PubMed](#)]
2. Novoselov, K.S.; Geim, A.K.; Morozov, S.V.; Jiang, D.; Katsnelson, M.I.; Grigorieva, I.V.; Dubonos, S.V.; Firsov, A.A. Two-dimensional gas of massless Dirac fermions in graphene. *Nature* **2005**, *438*, 197–200. [[CrossRef](#)] [[PubMed](#)]
3. Tang, Q.; Zhou, Z.; Chen, Z. Innovation and discovery of graphene-like materials via density-functional theory computations. *Wiley Interdiscip. Rev. Comput. Mol. Sci.* **2015**, *5*, 360–379. [[CrossRef](#)]
4. Neto, A.C.; Guinea, F.; Peres, N.M.; Novoselov, K.S.; Geim, A.K. The electronic properties of graphene. *Rev. Mod. Phys.* **2009**, *81*, 109. [[CrossRef](#)]
5. Novoselov, K.S.; Geim, A.K.; Morozov, S.V.; Jiang, D.; Zhang, Y.; Dubonos, S.V.; Grigorieva, I.V.; Firsov, A.A. Electric field effect in atomically thin carbon films. *Science* **2004**, *306*, 666–669. [[CrossRef](#)] [[PubMed](#)]
6. Kanoun, M.B.; Goumri-Said, S. Tailoring optoelectronic properties of monolayer transition metal dichalcogenide through alloying. *Materialia* **2020**, *12*, 100708. [[CrossRef](#)]
7. Chettri, B.; Patra, P.K.; Lalmuanchhana; Lalhriatzuala; Verma, S.; Rao, B.K.; Verma, M.L.; Thakur, V.; Kumar, N.; Hieu, N.N.; et al. Induced magnetic states upon electron–hole injection at B and N sites of hexagonal boron nitride bilayer: A density functional theory study. *Int. J. Quantum Chem.* **2021**, *121*, e26680. [[CrossRef](#)]
8. Raya, S.S.; Ansari, A.S.; Shong, B. Adsorption of gas molecules on graphene, silicene, and germanene: A comparative first-principles study. *Surf. Interfaces* **2021**, *24*, 101054. [[CrossRef](#)]
9. Lu, F.; Wang, W.; Luo, X.; Xie, X.; Cheng, Y.; Dong, H.; Liu, H.; Wang, W.-H. A class of monolayer metal halogenides MX₂: Electronic structures and band alignments. *Appl. Phys. Lett.* **2016**, *108*, 132104. [[CrossRef](#)]
10. Liu, P.; Lu, F.; Wu, M.; Luo, X.; Cheng, Y.; Wang, X.-W.; Wang, W.; Wang, W.-H.; Liu, H.; Cho, K. Electronic structures and band alignments of monolayer metal trihalide semiconductors MX₃. *J. Mater. Chem. C* **2017**, *5*, 9066–9071. [[CrossRef](#)]
11. Susner, M.A.; Chyasnachyus, M.; McGuire, M.A.; Ganesh, P.; Maksymovych, P. Metal thio- and selenophosphates as multifunctional van der Waals layered materials. *Adv. Mater.* **2017**, *29*, 1602852. [[CrossRef](#)]
12. Li, X.; Zhu, H. Two-dimensional MoS₂: Properties, preparation, and applications. *J. Mater.* **2015**, *1*, 33–44. [[CrossRef](#)]
13. Gurarlan, A.; Jiao, S.; Li, T.D.; Li, G.; Yu, Y.; Gao, Y.; Riedo, E.; Xu, Z.; Cao, L. Van der Waals force isolation of monolayer MoS₂. *Adv. Mater.* **2016**, *28*, 10055–10060. [[CrossRef](#)]
14. Molina-Sánchez, A.; Hummer, K.; Wirtz, L. Vibrational and optical properties of MoS₂: From monolayer to bulk. *Surf. Sci. Rep.* **2015**, *70*, 554–586. [[CrossRef](#)]
15. Sugita, Y.; Miyake, T.; Motome, Y. Multiple Dirac cones and topological magnetism in honeycomb-monolayer transition metal trichalcogenides. *Phys. Rev. B* **2018**, *97*, 035125. [[CrossRef](#)]
16. Chyasnachyus, M.; Susner, M.A.; Ievlev, A.V.; Eliseev, E.A.; Kalinin, S.V.; Balke, N.; Morozovska, A.N.; McGuire, M.A.; Maksymovych, P. Size-effect in layered ferroelectric CuInP₂S₆. *Appl. Phys. Lett.* **2016**, *109*, 172901. [[CrossRef](#)]
17. Zhang, X.; Zhao, X.; Wu, D.; Jing, Y.; Zhou, Z. MnPSe₃ monolayer: A promising 2d visible-light photohydrolytic catalyst with high carrier mobility. *Adv. Sci.* **2016**, *3*, 1600062. [[CrossRef](#)]
18. Jing, Y.; Zhou, Z.; Zhang, J.; Huang, C.; Li, Y.; Wang, F. SnP₂S₆ monolayer: A promising 2D semiconductor for photocatalytic water splitting. *Phys. Chem. Chem. Phys.* **2019**, *21*, 21064–21069. [[CrossRef](#)]
19. Liu, J.; Shen, Y.; Lv, L.; Wang, X.; Zhou, M.; Zheng, Y.; Zhou, Z. Rational design of porous GeP₂S₆ monolayer for photocatalytic water splitting under the irradiation of visible light. *Flatchem* **2021**, *30*, 100296. [[CrossRef](#)]
20. He, J.; Lee, S.H.; Naccarato, F.; Brunin, G.; Zu, R.; Wang, Y.; Miao, L.; Wang, H.; Alem, N.; Hautier, G.; et al. SnP₂S₆: A Promising Infrared Nonlinear Optical Crystal with Strong Nonresonant Second Harmonic Generation and Phase-Matchability. *ACS Photonics* **2022**, *9*, 1724–1732. [[CrossRef](#)]
21. Jacobsen, R.S.; Andersen, K.N.; Borel, P.I.; Fage-Pedersen, J.; Frandsen, L.H.; Hansen, O.; Kristensen, M.; Lavrinenko, A.V.; Moulin, G.; Ou, H.; et al. Strained silicon as a new electro-optic material. *Nature* **2006**, *441*, 199–202. [[CrossRef](#)] [[PubMed](#)]
22. Falvo, M.R.; Clary, G.J.; Taylor, R.M., II; Chi, V.; Brooks, F.P., Jr.; Washburn, S.; Superfine, R. Bending and buckling of carbon nanotubes under large strain. *Nature* **1997**, *389*, 582–584. [[CrossRef](#)]
23. Johari, P.; Shenoy, V.B. Tuning the electronic properties of semiconducting transition metal dichalcogenides by applying mechanical strains. *ACS Nano* **2012**, *6*, 5449–5456. [[CrossRef](#)]
24. Shi, H.; Pan, H.; Zhang, Y.W.; Yakobson, B.I. Quasiparticle band structures and optical properties of strained monolayer MoS₂ and WS₂. *Phys. Rev. B* **2013**, *87*, 155304. [[CrossRef](#)]
25. Horzum, S.; Sahin, H.; Cahangirov, S.; Cudazzo, P.; Rubio, A.; Serin, T.; Peeters, F.M. Phonon softening and direct to indirect band gap crossover in strained single-layer MoSe₂. *Phys. Rev. B* **2013**, *87*, 125415. [[CrossRef](#)]
26. Lee, Y.; Cho, S.B.; Chung, Y.C. Tunable indirect to direct band gap transition of monolayer Sc₂CO₂ by the strain effect. *ACS Appl. Mater. Interfaces* **2014**, *6*, 14724–14728. [[CrossRef](#)]
27. He, K.; Poole, C.; Mak, K.F.; Shan, J. Experimental demonstration of continuous electronic structure tuning via strain in atomically thin MoS₂. *Nano Lett.* **2013**, *13*, 2931–2936. [[CrossRef](#)] [[PubMed](#)]
28. Conley, H.J.; Wang, B.; Ziegler, J.I.; Haglund, R.F., Jr.; Pantelides, S.T.; Bolotin, K.I. Bandgap engineering of strained monolayer and bilayer MoS₂. *Nano Lett.* **2013**, *13*, 3626–3630. [[CrossRef](#)]

29. Yun, W.S.; Han, S.W.; Hong, S.C.; Kim, I.G.; Lee, J.D. Thickness and strain effects on electronic structures of transition metal dichalcogenides: 2H-MX₂ semiconductors ($M = \text{Mo}, \text{W}; X = \text{S}, \text{Se}, \text{Te}$). *Phys. Rev. B* **2012**, *85*, 033305. [[CrossRef](#)]
30. Zhong, F.; Wang, H.; Wang, Z.; Wang, Y.; He, T.; Wu, P.; Peng, M.; Wang, H.; Xu, T.; Wang, F.; et al. Recent progress and challenges on two-dimensional material photodetectors from the perspective of advanced characterization technologies. *Nano Res.* **2021**, *14*, 1840–1862. [[CrossRef](#)]
31. Wang, L.; Boutilier, M.S.H.; Kidambi, P.R.; Jang, D.; Hadjiconstantinou, N.G.; Karnik, R. Fundamental transport mechanisms, fabrication and potential applications of nanoporous atomically thin membranes. *Nat. Nanotechnol.* **2017**, *12*, 509–522. [[CrossRef](#)]
32. Zhao, J.; Ma, D.; Wang, C.; Guo, Z.; Zhang, B.; Li, J.; Nie, G.; Xie, N.; Zhang, H. Recent advances in anisotropic two-dimensional materials and device applications. *Nano Res.* **2021**, *14*, 897–919. [[CrossRef](#)]
33. Haborets, V.; Glukhov, K.; Banyas, J.; Vysochanskii, Y. Layered GeP₂S₆, GeP₂Se₆, GeP₂Te₆, SnP₂S₆, SnP₂Se₆, and SnP₂Te₆ Polar Crystals with Semiconductor–Metal Transitions Induced by Pressure or Chemical Composition. *Integr. Ferroelectr.* **2021**, *220*, 90–99. [[CrossRef](#)]
34. Lin, M.; Liu, P.; Wu, M.; Cheng, Y.; Liu, H.; Cho, K.; Wang, W.H.; Lu, F. Two-dimensional nanoporous metal chalcogenophosphates MP₂X₆ with high electron mobilities. *Appl. Surf. Sci.* **2019**, *493*, 1334–1339. [[CrossRef](#)]
35. Whangbo, M.H.; Brec, R.; Ouvrard, G.; Rouxel, J. Reduction sites of transition-metal phosphorus trichalcogenides MPX₃. *Inorg. Chem.* **1985**, *24*, 2459–2461. [[CrossRef](#)]
36. Togo, A.; Tanaka, I. First principles phonon calculations in materials science. *Scr. Mater.* **2015**, *108*, 1–5. [[CrossRef](#)]
37. Zhang, Y.; Wang, F.; Feng, X.; Sun, Z.; Su, J.; Zhao, M.; Wang, S.; Hu, X.; Zhai, T. Inversion symmetry broken 2D SnP₂S₆ with strong nonlinear optical response. *Nano Res.* **2022**, *15*, 2391–2398. [[CrossRef](#)]
38. Scalise, E.; Houssa, M.; Pourtois, G.; Afanas'ev, V.; Stesmans, A. Strain-induced semiconductor to metal transition in the two-dimensional honeycomb structure of MoS₂. *Nano Res.* **2012**, *5*, 43–48. [[CrossRef](#)]
39. Kohn, W.; Sham, L.J. Self-consistent equations including exchange and correlation effects. *Phys. Rev.* **1965**, *140*, A1133. [[CrossRef](#)]
40. Kresse, G.; Furthmüller, J. Efficient iterative schemes for ab initio total-energy calculations using a plane-wave basis set. *Phys. Rev. B* **1996**, *54*, 11169. [[CrossRef](#)]
41. Perdew, J.P.; Burke, K.; Ernzerhof, M. Generalized gradient approximation made simple. *Phys. Rev. Lett.* **1996**, *77*, 3865. [[CrossRef](#)] [[PubMed](#)]

Disclaimer/Publisher's Note: The statements, opinions and data contained in all publications are solely those of the individual author(s) and contributor(s) and not of MDPI and/or the editor(s). MDPI and/or the editor(s) disclaim responsibility for any injury to people or property resulting from any ideas, methods, instructions or products referred to in the content.